Research Square

Preprints are preliminary reports that have not undergone peer review.
They should not be considered conclusive, used to inform clinical practice,
or referenced by the media as validated information.

Mechanical Response to Tripping Impact and Multiphysics Coupling Analysis of the Drive Components in a High-speed Electromagnetic Repulsion Mechanical Switch

Yang Kuangbiao
Anhui University
Li Guoli
liguoli1224@163.com
Anhui University
Sun Zehui
Anhui University
Xu Jiazi
Anhui University
Ding Shuo
Anhui University

Research Article

Keywords: fast mechanical switch, electromagnetic repulsion mechanism, tripping impact, multiphysics coupling, finite element simulation, dynamic strain testing

Posted Date: November 26th, 2026

DOI: https://doi.org/10.21203/rs.3.rs-10933997/v1

License: This work is licensed under a Creative Commons Attribution 4.0 International License.
Read Full License

Additional Declarations: No competing interests reported.

Mechanical Response to Tripping Impact and Multiphysics Coupling Analysis of the Drive Components in a High-speed Electromagnetic Repulsion Mechanical Switch

Yang Kuangbiao[123] *Li Guoli**[123] *Sun Zehui*[13] *Xu Jiazi*[12] *Ding Shuo*[13]

（*1.School of Electrical Engineering and Automation, Anhui University Hefei 230601 China*

2.Engineering Research Center of Power Quality, Ministry of Education Hefei 230601 China

3.Anhui Key Laboratory of Industrial Energy Saving and Safety Hefei 230601 China

4.Anhui Collaborative Innovation Center of Industrial Energy Saving and Power Quality Control, Anhui University, Hefei 230601 China）

Correspondence: Prof. Guoli Li, Email: liguoli1224@163.com

Abstract

During the tripping phase, the integrated sealed electromagnetic-repulsion-type fast mechanical switch is subjected to millisecond-scale intense impact loads, which induce significant dynamic mechanical responses in transmission components and directly determine the operational reliability of the whole device. To address the limitation that single-physics-field simulation cannot fully reproduce the impact-induced mechanical behavior of the operating mechanism, this paper establishes mathematical models for the pulse-discharge circuit, transmission dynamics, and component dynamic response. A Multiphysics coupled simulation model is constructed based on COMSOL Multiphysics. Comparative simulations are carried out with respect to the material and thickness of the repulsion disc, the diameter of the lower tie rod, and the material of the insulated tie rod, to investigate the mechanical-response patterns of key transmission components under different structural and material conditions. A prototype is developed according to the parameter trends obtained from simulations, and a dynamic-strain testing platform is built. Strain gauges are mounted on critical stress-prone cross-sections of the insulated tie rod to capture the full-time-series dynamic stress during tripping. The engineering validity of the simulation model is verified by comparing prototype measured data against simulation outputs. The results show that adopting aerospace-grade aluminum 7075-T6 for the repulsion disc can effectively suppress component impact-induced deformation. Adjustments to repulsion-disc thickness and lower-tie-rod diameter significantly alter the mechanical response of the transmission system. Prototype tests yield a relative error of 2.9 % between simulated and measured peak stresses of the insulated tie rod, and the average error over the full time domain is below 7 %, which confirms that the presented multiphysics simulation method can effectively predict the impact mechanical behavior of physical prototypes. This work provides simulation guidance and experimental support for the structural design and engineering development of transmission components for fast mechanical switches.

Keywords: fast mechanical switch; electromagnetic repulsion mechanism; tripping impact; multiphysics coupling; finite-element simulation; dynamic strain testing

1. Introduction

With the large scale construction of flexible DC transmission and offshore renewable energy DC transmission projects, fault current limiting and rapid disconnection equipment for DC grids have become core components for ensuring the safe and stable operation of the system [1–2]. Hybrid DC circuit breakers, which combine the technical advantages of power electronic devices and fast mechanical switches, represent the mainstream technical solution for DC fault handling [3]; among these, the Thomson coil electromagnetic repulsion type fast mechanical switch, with its millisecond level response time, performs the critical task of rapidly separating the contacts during a fault. The mechanical reliability of the operating mechanism directly determines the operational performance of the entire circuit breaker [4–5].

During the tripping operation, the energy storage capacitor releases a large pulse current to the tripping coil. Eddy currents induced in the repulsion disc generate a brief, high amplitude electromagnetic repulsive force, driving the transmission chain comprising the repulsion disc, drive rod, and insulated tie rod to perform high-speed motion, thereby

achieving the effective contact gap within a few milliseconds [6–7]. Subjected to millisecond scale intense pulse impacts, transmission components deviate from ideal rigid-body motion. Impact loads excite stress-wave effects inside components and produce complex transient stress and structural-deformation responses. [8]. Insulated tie rods serve the dual functions of electrical isolation and mechanical force transmission; stress concentrations are prone to occur at structural transition points, making them highly susceptible to mechanical damage under repeated impact loads, and thus representing a weak link that limits the mechanical life of the entire unit [9]. Therefore, accurately capturing the impact mechanical response of key transmission components throughout the entire tripping process is of significant practical importance for the structural design and engineering development of prototypes.

In terms of analytical modeling of mechanisms, scholars both domestically and internationally have developed RLC discharge circuits and single degree of freedom analytical dynamic models, which can be used to predict the macroscopic motion characteristics of mechanisms. However, analytical models struggle to account for complex physical effects such as component flexibility, contact nonlinearity, and stress wave propagation, making it difficult to use them directly for the quantitative calculation of transient stresses in components [10–11]. Consequently, multiphysics finite-element simulation has been widely adopted in this research field. By solving for the coupled transient structural, electrical, and electromagnetic fields while simultaneously accounting for electromagnetic excitation, component flexibility, and contact boundaries it enables the numerical calculation of stress and deformation in repulsive mechanisms [12–13]. However, some existing studies have only conducted single field simulations of the electromagnetic field, neglecting the bidirectional coupling effects between the structural field and the electromagnetic field; as a result, the component stress results obtained from these simulations deviate significantly from those of actual prototypes [14].

At the experimental testing level, high-speed photography is commonly used to capture macroscopic motion parameters such as the displacement and velocity of the repulsion disc ; however, for sealed test specimens, where the drive rods and insulating rods are enclosed within the chamber, the stresses in internal components cannot be directly observed, making dynamic strain testing an effective method for obtaining transient impact stresses in these components [15–17]. Much of the existing simulation work often lacks experimental validation at the stress level using physical prototypes, and the stress time series generated by simulations lack support from measured data; while most literature focuses on multi objective parameter optimization, published research conducting systematic comparative analyses of the mechanical responses of transmission components under different materials and structural parameters remains limited [18–20].

In light of the current state of research described above, this paper focuses on the mechanical response of transmission components under trip impact. First, the operating mechanism of high-speed mechanical switches is explained, and a comprehensive analytical mathematical model is established that incorporates pulse discharge, electromagnetic repulsive force, transmission dynamics, and dynamic stresses in components; Second, a coupled finite-element model integrating circuit, electromagnetic field, and transient structural fields is constructed. Simulation comparisons are conducted across multiple sets of material and structural parameters to reveal the patterns of how parameter variations affect the mechanical response of the components. Based on the parameter patterns derived from the simulations, an engineering prototype is developed. Finally, dynamic strain tests are conducted using the prototype, and the engineering validity of the simulation model is verified using measured dynamic stress data, thereby providing support for the engineering design of transmission components in high-speed mechanical switches.

2. Working Principle of High-speed Mechanical Switches and a Mathematical Model of Component Stress

2.1. Overall Structure and Operating Principle of a High-speed Mechanical Switch

This paper focuses on a prototype of a monopole, integrated seal, electromagnetic repulsion rapid mechanical switch, which primarily consists of an energy storage capacitor, a repulsion drive coil, a metal repulsion disc, an insulated tie rod, upper and lower drive rods, moving and stationary contacts, contact disc springs, and a permanent magnet holding mechanism. The overall structure of the switch is shown in Fig .1.

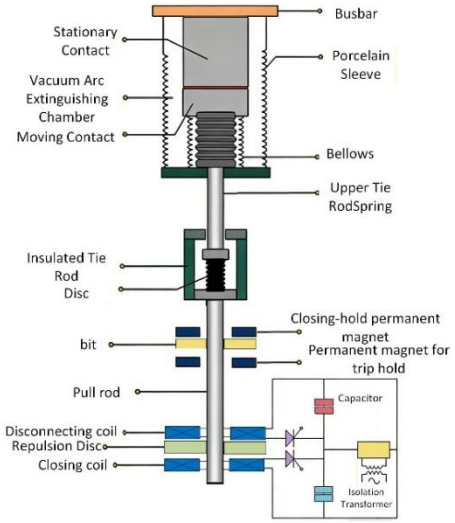


Fig. 1 Schematic Diagram of a High-speed Mechanical Switch

In the initial state, the moving and stationary contacts are in the closed position, and the disc spring is positioned at the junction of the insulator and the upper pull rod. To overcome the spring's reaction force and the weight of the moving parts, and to prevent accidental tripping caused by electrodynamic forces or mechanical vibrations, the magnetic force generated by the permanent magnet and the armature during the closed position must be in balance with the spring's reaction force. During opening, a thyristor triggers the energy storage capacitor to discharge into the opening coil. The pulse current induces eddy currents in the repulsion disc, creating an induced current opposite to the coil current, which in turn generates an electromagnetic repulsive force that drives the pull rod assembly. Once the overtravel is complete, the moving contact begins to move, achieving rapid opening.

The electromagnetic repulsive force generated during the circuit breaking process constitutes a short duration impact load, which is transmitted step by step along the repulsive force disc to the lower tie rod and the insulated tie rod. Stress concentrations occur at the structural transition points of the components; simultaneously, the impact load excites stress waves within the components, and the reflection and superposition of these stress waves further amplify local stress levels. As the core components for force transmission and electrical isolation, the insulated tie rods are subjected to the most severe impact stresses.

2.2. Mathematical Model of Stress in Switch Components

The dynamic impact stress excitation source for circuit breaker tripping originates from the electromagnetic driving force generated by capacitive pulse discharge. The mathematical model consists of four submodels: the pulse discharge circuit submodel, the electromagnetic field and force solver submodel, the transmission system dynamics submodel, and the component dynamic stress submodel.

2.2.1 Capacitor Discharge Circuit Model and Electromagnetic Force Solution Model

The trip drive uses capacitive pulse discharge to energize the excitation coil; the control equation for the external pulse discharge circuit is:

$$U_c(t) = L_c \frac{\mathrm{d}i(t)}{\mathrm{d}t} + R_c i(t) + \frac{1}{C}\int_0^t i(t)\mathrm{d}t \tag{1}$$

In the equation: Uc is the voltage across the capacitor, $i(t)$ is the discharge current, and L_c、R_c and C are the loop inductance, resistance, and capacitance, respectively.

The discharge current excites the excitation coil to generate a strong alternating magnetic field; eddy currents induced in the repulsion disc couple with the magnetic field to produce a pulsed electromagnetic repulsive force. The model neglects high frequency displacement currents and uses a low frequency transient electromagnetic field to solve for the global magnetic flux distribution. The electromagnetic driving force acting on the repulsion disc is determined by integrating the Maxwell stress tensor:

$$F_e = \frac{1}{2\mu_0}\oint_S (B^2 \cdot \boldsymbol{n} - 2(\boldsymbol{B} \cdot \boldsymbol{n})\boldsymbol{B})\mathrm{d}S \quad (2)$$

In the equation: F_e is the electromagnetic force acting on the repulsive disk; $\boldsymbol{B}$ is the magnetic flux density; $\boldsymbol{n}$ is the unit normal vector at the surface of the object; μ_0 is the magnetic permeability of free space; S is the closed integral surface of the repulsive disk.

2.2.2 Dynamic Model of the Transmission System

Using the time varying electromagnetic force F_e(t), obtained from the electromagnetic field solution, as the external driving load, and taking into account the equivalent moving mass, structural damping, nonlinear reaction forces from the disc springs, and frictional resistance of the moving pairs, we establish the second order dynamic control equations for the transmission system:

$$m_{eq}\frac{\mathrm{d}^2x(t)}{\mathrm{d}t^2} + c\frac{\mathrm{d}x(t)}{\mathrm{d}t} + kx(t) = F_e(t) - F_{spring}(x) - F_{friction}(x) \quad (3)$$

In the equation: m_{eq} is the equivalent mass of the moving part, c is the damping coefficient, k is the equivalent stiffness, F_{spring} is the contact spring reaction force, and $F_{friction}$ is the friction force.

Solving the above dynamic equation yields the displacement response $x(t)$ of the transmission system throughout the tripping process. The velocity $\dot{x(t)}$ and acceleration $\ddot{x(t)}$ of the mechanism can be further obtained by performing first and second-order differentiation on the displacement time-series. Based on force equilibrium, the time-varying impact load $F_{load}(t)$ acting on both ends of the insulated tie rod can be derived after deducting the spring reaction force and frictional resistance. This time-varying impact load serves as the direct external excitation that generates dynamic stress in the insulated tie rod.

2.2.3 Dynamic Stress Model for Insulated Tie Rods

The time varying impact load $F_{load}(t)$, derived from the dynamic analysis in the previous section, acts on both ends of the insulated tie rod. The stress at the critical cross section of the tie rod consists of a static component resulting from the preload of the disc spring, as well as a dynamic component resulting from the superposition of the impact load and the reflection of stress waves within the member. The expression for the dynamic stress at the critical cross section is:

$$\sigma(t) = \frac{F_{static}}{A} + \sigma_{dynamic}(t) \quad (4)$$

Where: F_{static} is the static load resulting from the preload of the disc spring; A is the effective cross sectional area of the critical section of the insulating tie rod; $\sigma_{dynamic}(t)$) is the time varying stress excited by $F_{load}(t)$ and including stress wave effects.

3. Multiphysics Co Simulation Design Method

During the operation of high-speed mechanical switches, key components are continuously subjected to impact loads. To conduct reliability research on high-speed mechanical switches, it is necessary to accurately capture the mechanical response of these key components. Currently, most studies are based on a single electromagnetic field and cannot comprehensively analyze the effects of stress and deformation during motion. Therefore, to address the aforementioned issues in the tripping process of high-speed mechanical switches, this study proposes a simulation method based on multiphysics coupling using COMSOL Multiphysics 6.4.

3.1. Simulation Model Development

The overall simulation approach is as follows: First, a simplified model of a high-speed mechanical switch is established and imported into the Electromagnetic Field module for electromagnetic field simulation; second, the Electromagnetic Field module is coupled with the Transient Structural Field module; and finally, a multiphysics analysis and solution for the electromagnetic field and transient structural field is performed. The simulation workflow is shown in Fig.2;

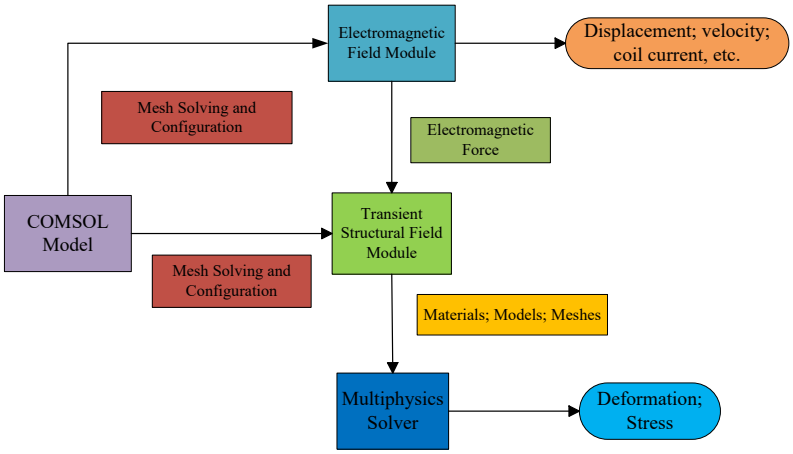


Fig.2 Block Diagram of the Coupled Multiphysics Simulation Model

First, in COMSOL, a motion model of the high-speed mechanical switch is created, as shown in Fig. 3. Next, the external circuit, materials, number of coil turns, boundary conditions, motion domain, and motion equations are configured, and a transient electromagnetic field solution is performed to obtain the displacement and velocity of moving parts such as the repulsion disc, the current in the trip coil, and the electromagnetic repulsive force acting on the repulsion disc. The electromagnetic repulsive force output from the electromagnetic field is coupled into the transient structural field solver, where meshing, component constraints, contact surface settings, and solver configuration are completed. This method enables internal data transfer between multiphysics fields, providing an effective approach for analyzing the structural reliability of high-speed mechanical switches.

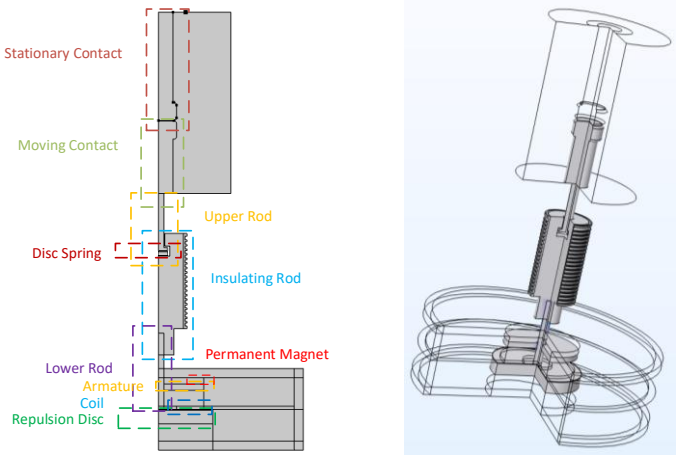


Fig. 3 2D axisymmetric model and 3D view of fast mechanical switch

4. Comparative Analysis of Multi Parameter Simulations

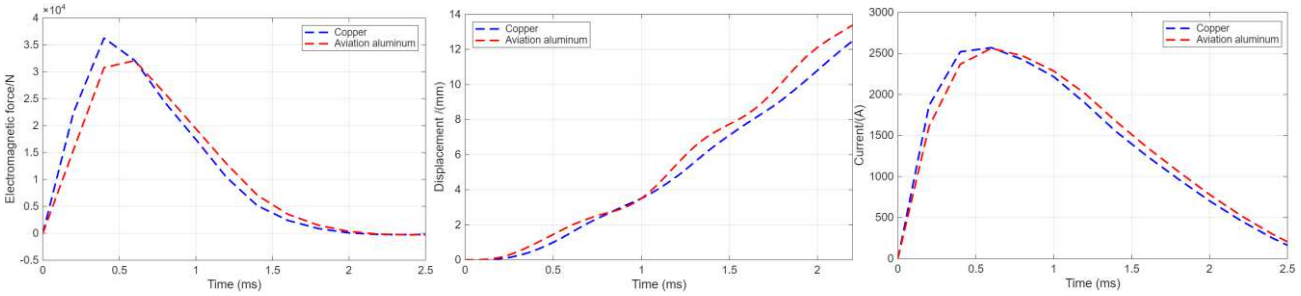
Based on the mathematical models of electromagnetic fields and the dynamics of the transmission system discussed earlier, it is evident that parameters such as voltage, resistance, current, mutual inductance, the mass of moving parts, and materials have a significant impact on the dynamic characteristics and operational reliability of high-speed mechanical switches. Therefore, this paper takes a 110 kV class high-speed mechanical switch with a total travel of 14 mm as the

research subject. Setting a breaking displacement of 6.5 mm and an overtravel of 1.5 mm to be achieved within 2 ms as performance constraints, a multi parameter simulation study is conducted from the perspectives of stress and deformation.

Based on engineering experience, the repulsion disc, lower tie rod, and insulated tie rod are subjected to severe alternating loads during the tripping impact, and their stress and deformation states directly determine the overall operational performance of the high-speed mechanical switch. Therefore, a comparative simulation analysis under different material and structural parameters was conducted focusing on these three key transmission components.

4.1. The Effect of Repulsion Disc Material

Repulsion discs made of different materials exhibit certain differences in magnetic permeability and electrical conductivity; these differences cause the repulsion discs to induce eddy currents of varying magnitudes. However, eddy currents of different magnitudes directly affect the electromagnetic repulsive force of the repulsion discs, which in turn affects the closing and opening processes of high-speed mechanical switches. At the same time, differences in the Young's modulus, Poisson's ratio, tensile strength, and compressive strength of different materials result in variations in the stresses and deformations generated by the repulsion disc during operation. With regard to the material of the repulsion disc, this paper selected two materials 7075 aerospace aluminum and red copper for simulation analysis; the results are shown in Fig. 4.



(a) Electromagnetic Force (b) Displacement (c) Current

Fig. 4 Effect of Material on Tripping Characteristics

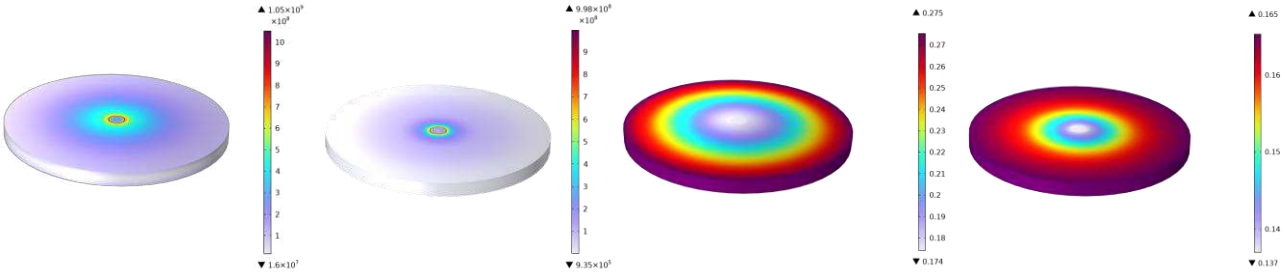
Simulation results show that, because the electrical conductivity of pure copper is higher than that of aerospace grade aluminum, the eddy current effect is more pronounced in the copper disc, resulting in a greater electromagnetic repulsive force 8.9% higher than that of the aluminum disc, at approximately 3,800 N. Although the copper disc is subjected to a larger electromagnetic force, its density is much higher than that of aluminum, significantly increasing the mass of the switch's moving parts. This results in a slower switch opening speed, with the displacement at 2 ms being lower than that of the aircraft grade aluminum; the peak excitation currents of the two are similar;

To couple the electromagnetic force solution results with the transient structural analysis, the material properties of 7075 aerospace aluminum and red copper such as Young's modulus, Poisson's ratio, tensile strength, and compressive strength were first defined. Differences in transient structural stress and deformation primarily depend on the tensile and compressive strengths of the different materials. The physical characteristics and mechanical property parameters of the two materials are shown in Table 1.

Table 1: Main Physical Characteristics and Mechanical Properties of Repulsion Discs

Parameters	Copper	Aerospace-grade aluminum 7075-T6
Density/(g·cm^{-3})	8.96	2.793
Young's modulus / GPa	113.6	71
Poisson's ratio	0.3	0.33
Tensile Strength/MPa	200~230	540
Compressive Strength/MPa	70~90	460

Fig.5 shows the simulation results for the stress and strain distributions of repulsive discs made of different materials.



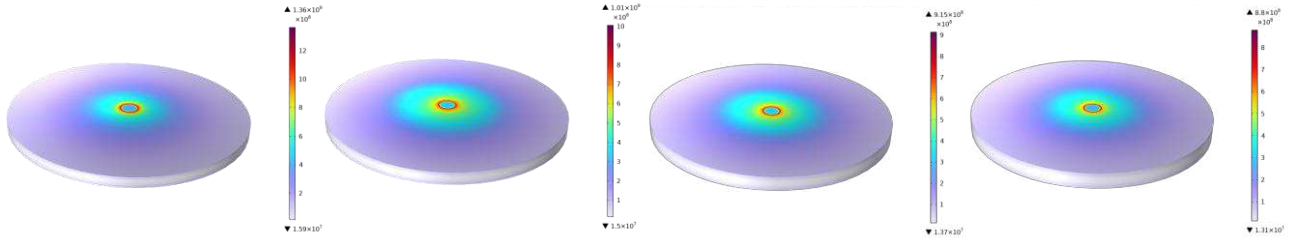
（a）Stress Distribution in Aircraft Grade Aluminum and Red Copper（b）Distribution of Deformation in Aircraft Grade Aluminum and Red Copper

Fig. 5 Stress and Strain Distribution in Repulsive Discs Made of Different Materials

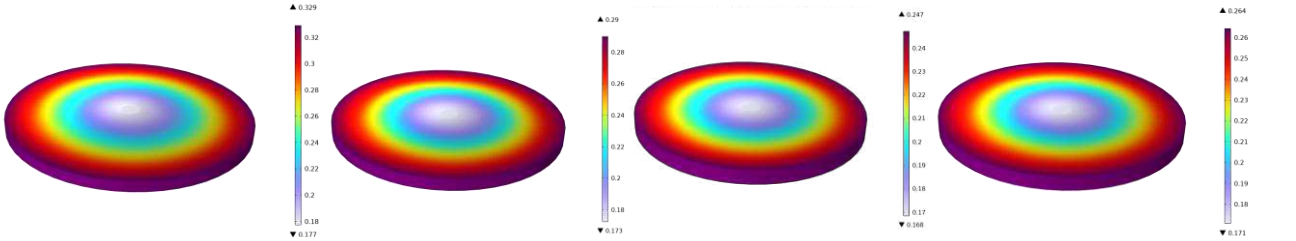
The simulation results show that when the repulsion disc is made of 7075 aerospace aluminum, the maximum deformation is 0.275 mm; when the material is red copper, the maximum deformation is 0.165 mm. The maximum von Mises stress obtained from the simulation occurs at the sharp corner of the center hole where the repulsion disc is assembled with the lower tie rod. This location is affected by stress singularities in the finite-element mesh, with local element stresses reaching 1.05 GPa and 0.998 GPa, respectively. These values at the local singular point are not used as a basis for evaluating the component's strength; Excluding the singular peak, the effective stress in the main body of the repulsion disc remains at the level of several hundred MPa. The central bore of the repulsion disc is a structurally weak area. Under repeated make-and-break cycles, this sharp corner is prone to stress-concentration-induced damage. Therefore, chamfer features should be introduced at this assembly hole in practical engineering prototypes to mitigate stress concentration. For both materials, the deformation at the edges of the repulsion disc remains within the elastic deformation range, so component failure will not occur; however, it may have some impact on the assembly fit of the transmission mechanism. After a comprehensive comparison of the dynamic characteristics during opening, component stress levels, and deformation states, aerospace grade aluminum was selected as the material for the ejection disc.

4.2. The Effect of Repulsion disc Thickness

Given that the inner and outer radii of the repulsion disc are fixed, the thickness of the repulsion disc affects its mass and tripping speed, which in turn influence its deformation and stress distribution. Therefore, a comparative simulation analysis was conducted using repulsion discs made of aerospace grade aluminum with thicknesses of 8 mm, 9 mm, 10 mm, and 11 mm. The results are shown in Fig. 6.



(a) Stress contour map of a repulsion disc with a thickness of 8–11 mm



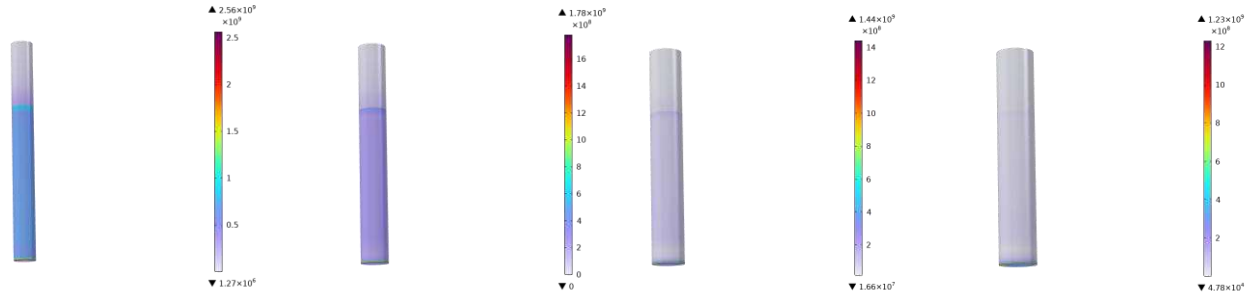
(b) Deformation contour map of an 8-11 mm thick repulsion disc

Fig. 6 Stress and Strain Distributions in Repulsion Discs of Different Thicknesses

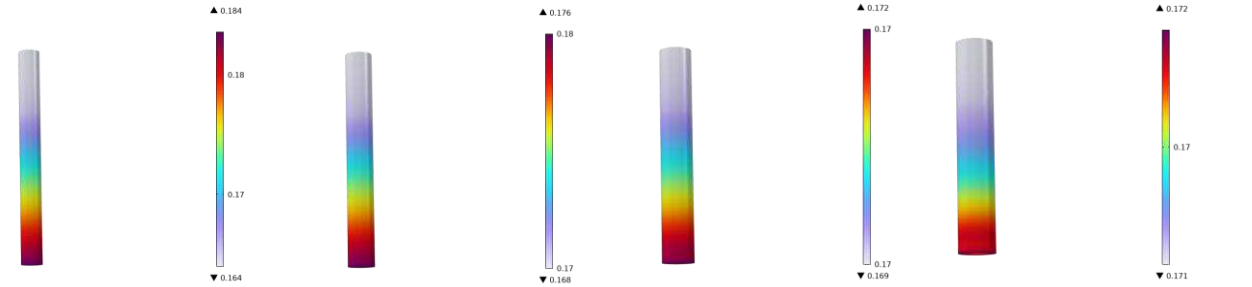
Simulation results reveal that the deformation of the repulsion disc decreases first and then increases with growing thickness, reaching its minimum value at a thickness of 10 mm. The maximum and minimum deformations of the repulsion disc across all simulated cases are 0.329 mm and 0.247 mm, respectively. The simulated peak stresses all appear at the sharp corner of the central hole where the repulsion disc assembles with the lower tie rod. Affected by finite-element-mesh-induced stress singularity, the stress of local elements ranges from 0.88 GPa to 1.36 GPa; such local singular-point values shall not be adopted for component strength assessment. After excluding singular peaks, the effective stress in the main body of the repulsion disc varies with thickness. The 10 mm-thickness case delivers optimal deformation performance, while the 11 mm-thickness case achieves the lowest effective stress in the disc main body, followed by the 10 mm case. Considering both deformation and main-body stress of the repulsion disc, 10 mm is selected as the design thickness of the repulsion disc.

4.3. The Effect of the Lower Link Diameter

When the thickness, outer diameter, inner diameter, and material of the repulsion disc remain constant, the diameter of the lower tie rod not only alters the stiffness and mass of the lower tie rod itself but also has a cascading effect on the stress strain state of the insulated tie rod to which it is assembled. In this section, using aerospace grade aluminum 7075 as the material for the lower tie rod, simulation analyses were conducted with four sets of diameter parameters 14 mm, 15 mm, 16 mm, and 17 mm to determine the stress and strain distribution in the lower tie rod itself, as well as its impact on the insulated tie rod; the simulation results are shown in Fig.7.



(a) Stress contour map of a lower tie rod with a diameter of 14–17 mm



(b) Deformation cloud diagram of a pull rod with a diameter of 14–17 mm

Fig. 7 Deformation and Stress Distribution in Tension Rods of Different Diameters

Simulation results indicate that a change in the diameter of the lower tie rod directly affects the sectional stiffness of the component and simultaneously causes a change in the moment of inertia of the entire transmission system; as the diameter of the lower tie rod increases, not only does the stress level of the lower tie rod itself change, but the stresses and deformations of associated components such as the insulating tie rod and repulsion disc also change in tandem. As shown in the simulation results in Fig.7, the deformation and stress of the lower tie rod do not exhibit a monotonic relationship with diameter: when the diameter is 14 mm, both the maximum deformation and maximum stress of the lower tie rod reach

their peaks; as the diameter continues to increase, the maximum stress in the pull rod gradually decreases, but the deformation does not decrease monotonically with increasing diameter; it is not until the diameter reaches 16 mm that the component achieves its minimum deformation. An excessively small rod diameter results in insufficient component stiffness and considerable deformation under impact loads. By contrast, an overly large diameter improves rod-body stiffness but raises the total mass of moving parts, further increasing the impact load acting on the downstream repulsion disc.

The effect of the lower tie rod on the stress in the insulating tie rod is primarily concentrated at the assembly connection point in the upper section, where stress concentration is significant and which is a critical area prone to damage in the insulating tie rod. Therefore, during the engineering design process, it is necessary to consider both the strength of the lower tie rod itself and the additional impact effects that changes in diameter have on the repulsion disc and the insulating tie rod. Fig.8 shows the overall stress distribution in the insulating tie rod under the action of lower tie rods of different diameters.

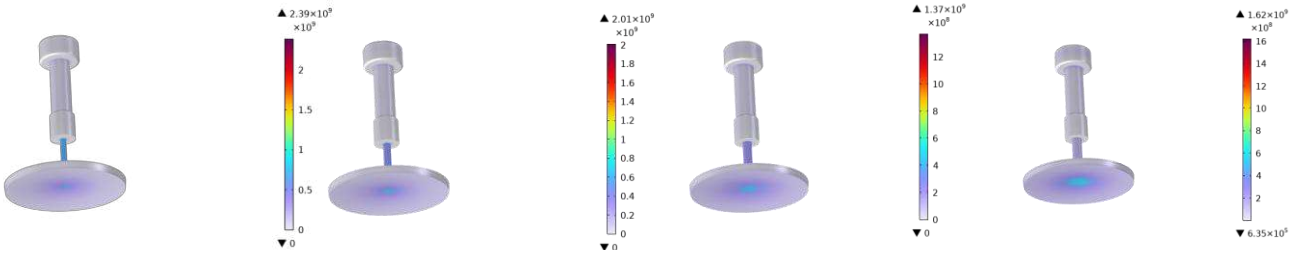
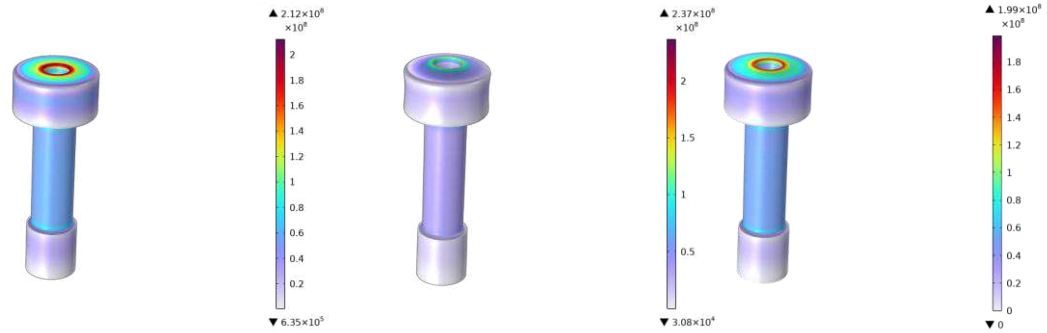


Fig. 8 Stress distribution generated by pull rods with diameters of 14 mm, 15 mm, 16 mm, and 17 mm on the repulsion disc and insulated tie rod

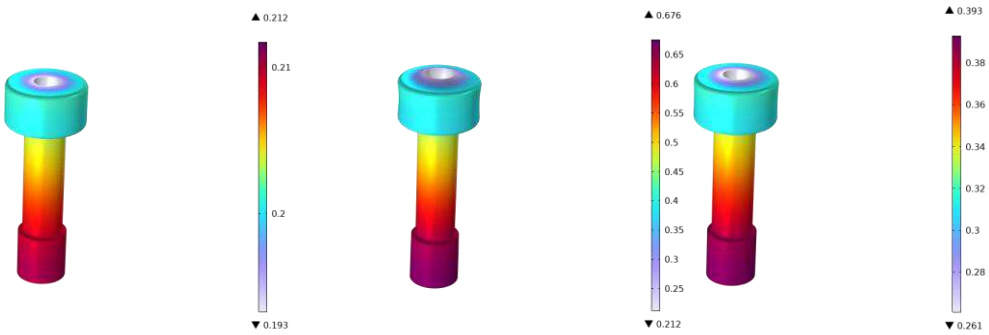
The overall structural stress does not follow a monotonic variation pattern as the diameter of the lower tie rod increases. The deformation and stress of the tie rod reach their peak under a 14 mm diameter condition; as the diameter continues to increase, the stress level decreases slightly until the component achieves minimum deformation at a diameter of 16 mm. Taking into account the deformation and stress of the lower tie rod, as well as the coupled effects on the insulating tie rod and the repulsion disc, the lower tie rod diameter for this 110 kV rapid mechanical switch was determined to be 16 mm.

4.4. The Effect of Insulated Tie Rod Material on Stress and Deformation

Insulated tie rods serve the dual functions of transmitting mechanical forces and providing electrical isolation; the material properties directly determine the structural response under impact conditions. In this section, three insulating materials carbon fiber CFRP, nylon 11, and epoxy resin X238 were selected for simulation comparisons. Fig. 9 shows the stress and strain contour plots for insulated tie rods made of different materials.



(a) Stress contour plots for CFRP, nylon, and X238



(b) Strain maps for CFRP, nylon, and X238

Fig. 9 Stress and Strain Distribution in Insulated Tie Rods Made of Different Materials

There are significant differences in the elastic modulus and mechanical strength among different insulating materials; under the same impact load, the stress amplitude and degree of deformation of the tie rods vary. Simulation results show that the maximum stress value of the nylon insulating tie rod is 0.237 GPa; CFRP had the second highest stress value; CFRP has higher stiffness and exhibits less deformation under the same impact load; Nylon 11 has better toughness, but the component's deformation is relatively large, resulting in more significant displacement fluctuations under high frequency repetitive impact conditions. After comprehensively considering the deformation and stress results of the insulating rods, CFRP was selected as the material for the insulating rods.

5. Testing and Verification of the Dynamic Characteristics of High-speed Mechanical Switches

Based on the parameter trends obtained from the multiple sets of simulations described above, the key design parameters for the prototype were determined, and a physical prototype of a 110 kV fast mechanical switch was developed. The prototype parameters are shown in Table 2, and a physical view of the prototype is shown in Fig.10.

Table 2: Parameters of the High-Speed Mechanical Switch Prototype

Project Name	Parameters
Repulsion Disc Material	Aerospace-grade aluminum 7075-T6
Number of radial turns on the repulsion disc	24
Repulsion Disc Thickness / mm	10
Stroke/mm	14
Trip Time/ms	2
Energy Storage Capacitor / mF	4
Lower Link Diameter / mm	16
Insulated Rod Material	Carbon Fiber CFRP



Fig. 10 Physical Prototype of a High-Speed Mechanical Switch

5.1. Test Platform and Measurement Point Layout

The test prototype is the main body of a 110 kV class high-speed mechanical switch; the test system includes a charging power supply, a pulse energy storage capacitor, a thyristor triggering control system, a camera module, and a high-speed dynamic strain acquisition module. The camera module uses a Qian yan lang NEO20 high-speed camera, configured with a sampling frame rate of 10,000 frames/s and an image resolution of 1280 × 800 pixels; the camera's optical axis is positioned perpendicular to the plane of motion of the ejection disc, providing complete coverage of the disc's full stroke. The high-speed dynamic strain acquisition module uses an NI 9923 data acquisition system; the system's test setup is shown in Fig. 11.

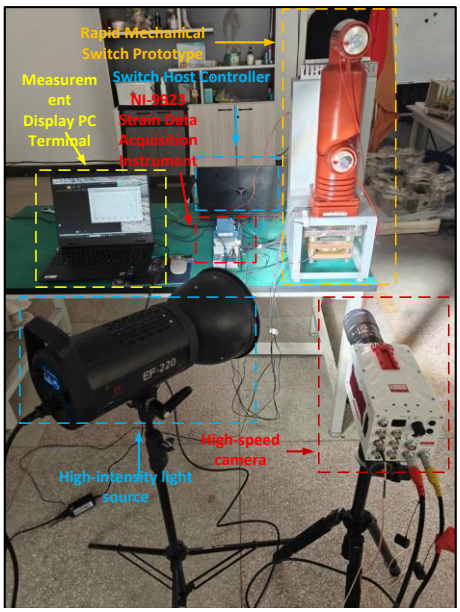


Fig. 11 Test Setup for the Stress Data Acquisition System of the High-Speed Mechanical Switch Prototype

Based on the stress distribution obtained from simulations, displacement data acquisition and dynamic strain and stress measurements were conducted using the test platform, with strain gauges installed at critical sections of key components. The transition point of the insulated tie rod structure is a critical section prone to stress concentration; axial strain gauges were applied at this location. Proper insulation and vibration protection for the strain gauges were ensured. Details of the strain gauge installation are shown in Fig. 12.

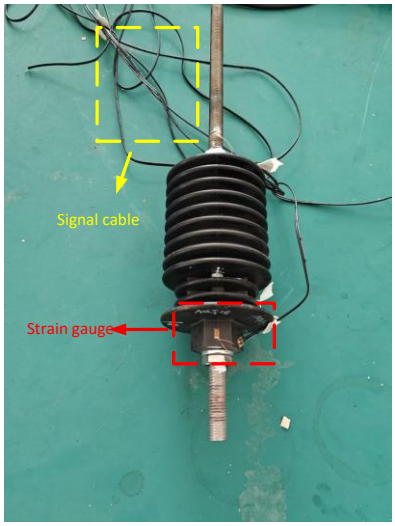


Fig.12 Detailed view of strain gauge placement at vulnerable locations on an insulated tie rod

The entire tripping process is divided into five time sequence phases. Using the moment the controller issues the tripping command as the reference time, the time boundaries for each phase are shown in Figure 13;

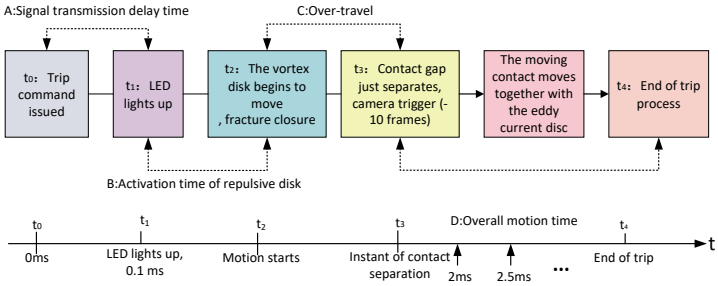


Fig. 13 Schematic diagram of the opening test process

1) At time t_0: The controller issues a disconnection command, marking the start of the test. The interval from t_0 to t_1 represents the signal transmission delay; during this period, the high-speed camera cannot capture valid motion signals, so this interval is set to 0.1 ms.

2) Time t_1: The LED illuminates; the solid state relay begins to conduct; the capacitor begins to discharge; and the current in the drive coil begins to rise. The period from t_1 to t_2 is the eddy current disc startup phase. During this period, the electromagnetic force is not yet sufficient to overcome static friction and the spring preload, so the repulsion disc remains stationary.

3) At time t_2: The repulsion disc begins to move, marking the start of the overtravel phase. The period from t_2 to t_3 is the overtravel phase, during which the repulsion disc drives the pull rod to move, but the moving contact has not yet separated from the stationary contact. Due to a 1 ms hardware debounce delay in the high-speed camera's triggering, the selection of the actual valid image sequence must be shifted back by 10 frames from the trigger time.

4) At time t_3: This marks the moment of initial separation, when the moving and stationary contacts become electrically separated, and the overtravel phase ends. The period from t_3 to t_4 constitutes the integrated motion phase, during which the repulsion disc and the moving contact move together with the pull rod until the breaking process is complete.

5) At time t_4: The breaking process is complete.

Image processing is based on the LabVIEW Vision Module. The processing workflow consists of the following steps: image import, region selection, threshold segmentation, center of mass calculation, and output of a time series displacement curve to track the measured displacement of the repulsion disc . An example of image processing for high-speed camera target tracking is shown in Fig. 14.

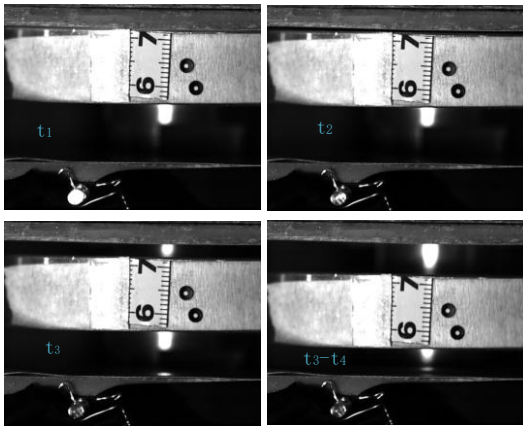


Fig.14 Example of Image Processing for Target Tracking Using a High-Speed Camera

Under circuit breaking conditions, the insulating tie rod primarily experiences axial tensile force, which is predominantly uniaxial; Hooke's law is used to convert strain into stress time series;

$$\sigma(t) = E\varepsilon(t) \tag{5}$$

$\sigma(t)$ is the instantaneous stress at time t (MPa); E is Young's modulus; $\varepsilon(t)$ is the instantaneous strain measured by the strain gauge;

To improve signal reliability, the raw strain signals collected during the experiment underwent targeted preprocessing: first, localized distorted values were removed from the data; then, bandpass filtering and local averaging were applied to smooth out the strain variations, thereby effectively improving signal quality. Using a typical operating condition with a rated voltage of 800 V, the simulated stress time series at the critical cross section was compared with the measured stress time series on the same time axis; the results are shown in Fig.15.

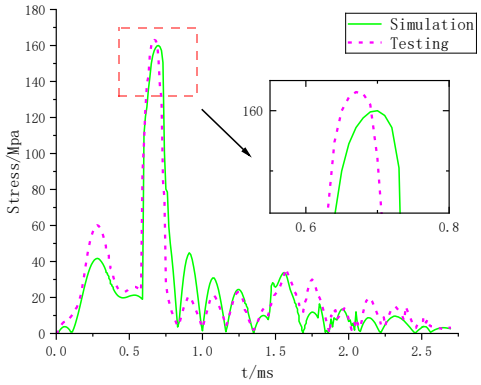


Fig.15 Comparison of Simulated and Measured Stresses in an Insulated Tie Rod

The test results show that the measured peak stress of the insulated tie rod was 167 MPa, while the peak stress obtained from the simulation was 162 MPa, resulting in a relative error of 2.9% at the peak. The average relative error across the entire time domain was less than 7%. In terms of temporal response characteristics, the first stress peak appeared at 0.3 ms, the global maximum stress was reached at 0.6 ms, and the stress subsequently exhibited an oscillatory decay pattern. The simulation and experimental curves were generally consistent in terms of the onset of the stress rise, the timing of the peak, and the oscillatory decay trend.

6. Conclusion

1. A complete set of analytical mathematical models, including pulse discharge circuit description, electromagnetic repulsion solving, transmission system dynamics, and component dynamic response, is established for millisecond scale intense tripping impacts of integrated sealed fast mechanical switches. A Multiphysics coupled finite-element model is built to calculate the mechanical responses of key transmission components.

2. Comparative simulations are performed for multiple material-structure parameter combinations of the repulsion disc, lower tie rod, and insulated tie rod. The simulation results indicate that aerospace-grade aluminum 7075-T6 for the repulsion disc can effectively mitigate impact caused component deformation. Variations in repulsion-disc thickness and lower-tie-rod diameter alter both component stiffness and overall system inertia and further change the mechanical-response characteristics of the whole transmission chain.

3. A physical prototype is developed guided by simulation-derived parameters. A dynamic strain test platform is constructed, and strain gauges are arranged on critical stress prone cross-sections of the insulated tie rod for repeated tripping tests. Under typical working conditions, the relative error between simulated and measured peak stress reaches 2.9 %, and the full time domain average error is less than 7 %, with high consistency in stress time series characteristics. Prototype measurements verify that the proposed multiphysics simulation model can accurately predict the impact mechanical behavior of physical prototypes. The presented simulation analysis workflow possesses practical engineering value and can provide simulation basis and experimental references for the R&D and design of transmission components for similar fast mechanical switches.

References

[1] Franck, C. M. (2011). HVDC circuit breakers: A review identifying future research needs. IEEE transactions on power delivery, 26(2), 998 1007.

[2] Shi, J., Mo, Y., Su, H., Ju, S., Tan, T., Jia, R., ... & Jia, S. (2025). Study on the drawn vacuum arc characteristics of the 126 kV axial magnetic field contacts. IEEE Transactions on Plasma Science, 53(7), 1592 1603.

[3] Bissal, A., Magnusson, J., & Engdahl, G. (2012). Comparison of two ultra fast actuator concepts. IEEE Transactions on Magnetics, 48(11), 3315 3318.

[4] Bissal, A., Magnusson, J., & Engdahl, G. (2015). Electric to mechanical energy conversion of linear ultrafast electromechanical actuators based on stroke requirements. IEEE Transactions on Industry Applications, 51(4), 3059 3067.

[5] Liu, Z., Xiu, S., Wang, T., Zhao, L., Zhang, Y., & Li, R. (2019). Experimental and simulation research on influence of axial magnetic field components on vacuum arc between transverse magnetic field contacts. IEEE Transactions on Plasma Science, 47(3), 1648 1656.

[6] Vilchis Rodriguez, D. S., Shuttleworth, R., & Barnes, M. (2017). Modelling thomson coils with axis symmetric problems: practical accuracy considerations. IEEE Transactions on Energy Conversion, 32(2), 629 639.

[7] Peng, C., Husain, I., Huang, A. Q., Lequesne, B., & Briggs, R. (2016). A fast mechanical switch for medium voltage hybrid DC and AC circuit breakers. IEEE Transactions on Industry Applications, 52(4), 2911 2918.

[8] Zhu, Z., Yuan, Z., Chen, L., He, J., & Zhu, Z. (2020). Vibration characteristics of thomson coil actuator based on simulation and experiments. IEEE Transactions on Energy Conversion, 35(3), 1228 1237.

[9] Li, M., Gong, P., Wu, Y., & Wu, Y. (2020). Analysis of structure strength for direct current high-speed switch based on flexible body theory. Advances in Mechanical Engineering, 12(3), 1687814020912984.

[10] Sim, M. S., Bukhari, S. S. H., & Ro, J. (2022). Analysis and design of a Thomson coil actuator system for an HVDC circuit breaker. IEEE Access, 10, 58354 58359.

[11] Al Dweikat, M., Cui, J., Sun, S., Yang, M., Zhang, G., & Geng, Y. (2022, June). A review on Thomson coil actuators in fast mechanical switching. In Actuators (Vol. 11, No. 6, p. 154). MDPI.

[12] Rodak, M., & Borkowski, P. (2024). Analysis of Circuits Supplying Thomson Coil Actuator Operating in Vacuum Contact Units of DC and AC Ultra Fast Circuit Breakers. Energies, 17(22), 5809.

[13] Yang, W., Fansong, M., & Guofu, Z. (2026). Collaborative Optimization of Dynamic Characteristics and Armature Structural Safety in Electromagnetic Repulsion Mechanisms. Energies, 19(15), 3665.

[14] Ding, C., Ding, Y., Yuan, Z., & Li, J. (2023). Structural optimization design of electromagnetic repulsion mechanism based on BP neural network and NSGA-II. IEEJ Transactions on Electrical and Electronic Engineering, 18(12), 1914 1922.

[15] Wu, Y., Wu, Y., Rong, M., Yang, F., Zhong, J., Li, M., & Hu, Y. (2015). A new Thomson coil actuator: Principle and analysis. IEEE Transactions on Components, Packaging and Manufacturing Technology, 5(11), 1644 1655.

[16] Cui, P., Li, G., Sun, Z., Xu, J., Zhang, G., Chen, Z., & Guan, W. (2025). Finite-element joint simulation model applied to fast mechanical switching of controlled resonance combination circuit breakers. High Voltage, 10(2), 419 435.

[17] Niu, M., Xia, J., & Yong, H. (2021). Numerical analysis of the electromechanical behavior of high field REBCO coils in all superconducting magnets. Superconductor Science and Technology, 34(11), 115005.

[18] Xiu, S., Wang, J., Jiang, Y., Wei, L., An, M., & Liu, S. (2025). Investigation of vacuum arc root characteristics between transverse magnetic field contacts with slot structure. Physics of Plasmas, 32(7).

[19] Zhou, Y., Huang, Y., Wen, W., Yang, C., Liu, B., Hu, M., & Bai, Y. (2019, August). Effect of Voltage on Thomson Coil Actuator for Fast Mechanical Switch. In The International Symposium on High Voltage Engineering (pp. 1349 1358). Cham: Springer International Publishing.

[20] Yao, X., Guan, C., Wang, J., Geng, Y., Liu, Z., & Zhai, X. (2021). Optimizing the opening velocity for a vacuum circuit breaker with cup type axial magnetic field contacts. IEEE Transactions on Plasma Science, 49(5), 1636 1647.

Acknowledgements

Funding: This work was supported by the Anhui Provincial Science and Technology Tackling Plan (Grant No. 202423i08050047).

CRediT author statement

Conceptualization: Yang Kuangbiao, Li Guoli; Data curation: Yang Kuangbiao, Sun Zehui; Formal analysis: Yang Kuangbiao, Xu Jiazi; Funding acquisition: Li Guoli; Investigation: Yang Kuangbiao, Ding Shuo; Methodology: Yang Kuangbiao, Li Guoli; Project administration: Li Guoli; Resources: Li Guoli; Software: Yang Kuangbiao, Xu Jiazi; Supervision: Li Guoli; Validation: Yang Kuangbiao, Sun Zehui; Visualization: Yang Kuangbiao, Ding Shuo; Writing – original draft: Yang Kuangbiao; Writing – review & editing: Li Guoli.

Data availability

The datasets generated and analysed during the current study are not publicly available due to institutional restrictions, but are available from the corresponding author on reasonable request.

Conflict of Interest

Conflict of Interest: The authors declare that they have no known competing financial interests or personal relationships that could have appeared to influence the work reported in this paper.